JOC Article
pubs.acs.org/joc

Conformational Effects Induced by Guest Encapsulation in an Enantiopure Water-Soluble Cryptophane

Aude Bouchet,[†] Thierry Brotin,*[,‡] Mathieu Linares,[§] Hans Ågren,[§] Dominique Cavagnat,[†] and Thierry Buffeteau*[,†]

[†]*Institut des Sciences Moléculaires (UMR 5255 − CNRS), Université Bordeaux 1, 351 Cours de la Libération, 33405 Talence, France,* [‡]*Laboratoire de Chimie de l'ENS-LYON (UMR 5182 − CNRS), Ecole Normale Supérieure de Lyon, 46 Allée d'Italie, 69364 Lyon 07, France, and* [§]*Department of Theoretical Chemistry, School of Biotechnology, Royal Institute of Technology, S-106 91 Stockholm, Sweden*

t.buffeteau@ism.u-bordeaux1.fr; thierry.brotin@ens-lyon.fr

Received November 25, 2010

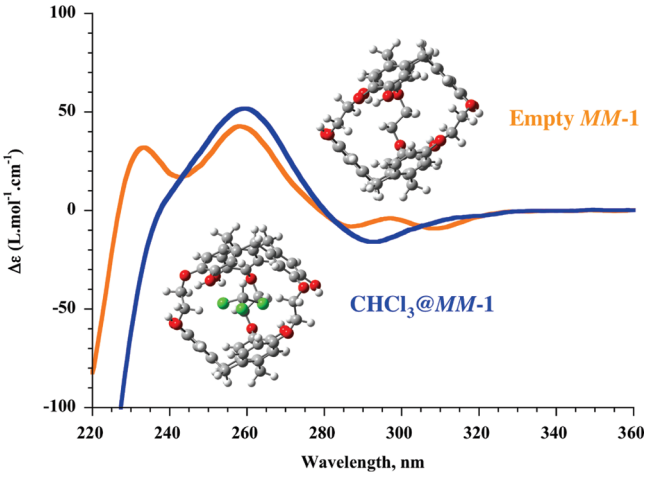

A new water-soluble cryptophane **1** derivative (penta-hydroxyl cryptophane-A) has been synthesized from cryptophanol-A and the chiroptical properties of its two enantiomers *MM*-**1** and *PP*-**1** have been studied by polarimetry, electronic circular dichroism (ECD), and vibrational circular dichroism (VCD). Cryptophane **1** shows specific circular dichroism responses upon complexation that depend on the size of the guest and on the nature of the counterion (Li^+, Na^+, K^+, Cs^+) present in the solution. In LiOH and NaOH solutions, chiroptical changes induced by the encapsulation of guests and by the presence of cations in the vicinity of hosts can be interpreted from molecular dynamics (MD) and ab initio calculations by subtle conformational changes of the bridges. In KOH solution, the exchange dynamics is dependent on the size of the guest molecules, whereas in CsOH solution no encapsulation effect is observed whatever the size of the guest molecule. This last behavior comes from the fact that host **1** exhibits a very high affinity for cesium cations.

Introduction

In a series of recent papers, we have investigated the chiroptical properties of several cryptophane molecules by polarimetry, electronic circular dichroism (ECD) and vibrational circular dichroism spectroscopy (VCD).[1] These studies were motivated because cryptophane derivatives possess interesting binding properties that can be evidenced by chiroptical techniques. Indeed, the ability of cryptophanes to bind small organic molecules or atoms like xenon appears promising to design sensor devices or magnetic resonance imaging biosensor in combination with hyperpolarized xenon.[2] This feature is the consequence of the tridimensional

(1) (a) Brotin, T.; Cavagnat, D.; Dutasta, J. P.; Buffeteau, T. *J. Am. Chem. Soc.* **2006**, *128*, 5533–5540. (b) Cavagnat, D.; Buffeteau, T.; Brotin, T. *J. Org. Chem.* **2008**, *73*, 66–75. (c) Brotin, T.; Cavagnat, D.; Buffeteau, T. *J. Phys. Chem. A* **2008**, *112*, 8464–8470. (d) Bouchet, A.; Brotin, T.; Cavagnat, D.; Buffeteau, T. *Chem.—Eur. J.* **2010**, *16*, 4507–4518.

Published on Web 01/26/2011 DOI: 10.1021/jo102350g

structure of cryptophanes that creates a lipophilic cavity suitable for accommodating small neutral molecules.[3] The specific molecular recognition is mainly determined by the internal volume of the cavity that in turn is controlled by the length of the aliphatic linkers (81 $Å^3$, 95 $Å^3$ and 121 $Å^3$ for methoxy, ethoxy, and propoxy linkers, respectively) that connect the two cyclotriveratrylene (CTV) bowls.[3b]

Beside their interesting binding properties, some cryptophane molecules such as the cryptophane-A congeners are inherently chiral derivatives that can be resolved from known experimental procedures with excellent enantiomeric excess.[4] For instance, enantiopure cryptophane-A congeners can be obtained from enantiopure cryptophanol in fair amounts (0.1−0.5 g), allowing a complete study of their chiroptical properties by polarimetry as well as ECD and VCD spectroscopies. The results obtained by these techniques have revealed that the chiroptical properties of cryptophane-A are strongly dependent on some external parameters such as the nature of the solvent and the ability of a guest molecule to enter the cavity. Moreover, the VCD results associated with ab initio calculations at the density functional theory (DFT) level have clearly shown that the observed spectral modifications are associated with subtle conformational modifications of the linkers occurring during the encapsulation process.[1a−c] This behavior has been revealed for cryptophanes with C_1-symmetry which exhibit a preferential *gauche*−*trans*−*trans* conformation of the three linkers.[1b,c] Thus, the guest-free cryptophane (hereafter called "empty")[5] favors the *gauche* conformation of the bridges in order to reduce the size of the inner cavity (hydrophobic effect), whereas the filled cryptophane favors the *trans* conformation of the linkers when large guest molecules, such as CH_2Cl_2 or $CHCl_3$ enter its cavity. On the other hand, significant ECD and VCD spectral modifications have been observed for the water-soluble cryptophane-A bearing six hydroxyl functions, depending on the pH conditions, the nature of the guest, as well as the nature of the counterions.[1d]

SCHEME 1. Structure of Compounds 1 and 2 (Only *MM* Enantiomer is Shown)

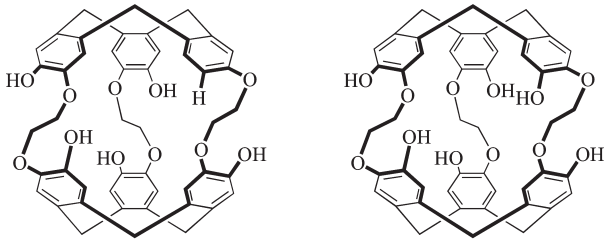

MM-**1** *MM*-**2**

Herein, we wish to study the influence of the symmetry of a water-soluble cryptophane on its overall chiroptical properties. Indeed, as previously observed for cryptophane-A derivatives in organic solution,[1b,c] the breakdown of symmetry of the water-soluble hexa-hydroxyl cryptophane-A (having D_3- or C_3-symmetry depending on the conformation of the bridges) is expected to induce large modifications of the ECD and VCD spectra upon guest encapsulation. Thus, the penta-hydroxyl cryptophane-A derivative, **1**, has been synthesized and differs from the hexa-hydroxyl cryptophane-A, **2**, by a single hydrogen atom replacing a hydroxyl function (see Scheme 1). This chemical transformation not only modifies the electronic distribution but also creates a larger window in one of the three portals of the host molecule.

We describe in this article the synthesis of the new water-soluble cryptophane **1** derivative. The chiroptical properties of its two enantiomers *MM*-**1** and *PP*-**1** were investigated in water under basic conditions (pH > 12) by polarimetry, electronic circular dichroism and vibrational circular dichroism. The effects of the pH, the nature of the counterions and the size of the guest molecules on the chiroptical properties of host **1** have been thoroughly studied. Finally, a conformational analysis of empty *PP*-**1** and $CHCl_3$@*PP*-**1** complex has been performed using molecular dynamics (MD) and DFT calculations to support the experimental results.

Results

Synthesis of Enantiopure Penta-Hydroxyl Cryptophane-1. The synthetic route used to obtain water-soluble penta-hydroxyl cryptophane, *rac*-**1** and its two enantiomers *MM*-**1** and *PP*-**1** from cryptophanol *rac*-**3** and its two enantiomers *MM*-**3** and *PP*-**3** is presented in Scheme 2. Cryptophanol-**3** was allowed to react with anhydride triflic and then with a palladium catalyst to give rise to cryptophanes *rac*-**4**, *MM*-**4** and *PP*-**4**.[1c] The removal of the five methyl groups was carried out in THF in presence of an excess of freshly prepared lithium diphenylphosphide (1M) according to an experimental procedure previously reported for the synthesis of compound **2**.[1d] This synthetic route provides *rac*-**1** and the two enantiomers *MM*-**1** and *PP*-**1** in 70%, 76% and 73% yields, respectively. An additional purification step was carried out by reacting *rac*-**1**, *MM*-**1** and *PP*-**1** with anhydride acetic in pyridine to provide new derivatives *rac*-**5**, *MM*-**5** and *PP*-**5** in 73%, 75%, 79% yields, respectively. According to Pr. V. Prelog specifications

(2) (a) Goodson, B. M. *J. Magn. Reson.* **2002**, *155*, 157–216. (b) Cherubini, A.; Bifone, A. *Prog. Nucl. Magn. Reson. Spectrosc.* **2003**, *42*, 1–30. (c) Oros, A. M.; Shah, N. J. *Phys. Med. Biol.* **2004**, R105. (d) Schröder, L.; Lowery, T.; Hilty, C.; Wemmer, D.; Pines, A. *Science* **2006**, *314*, 446–449. (e) Berthault, P.; Bogaert-Buchmann, A.; Desvaux, H.; Huber, G.; Boulard, Y. *J. Am. Chem. Soc.* **2008**, *130*, 16456–16457.

(3) (a) Collet, A. *In Comprehensive Supramolecular Chemistry*; Atwood, J. L., Davis, J. E. D., MacNicol, D. D., Vögtle, F., Eds. ; Pergamon Press: New York, 1996; Vol. 2, Chapter 11, pp 325−365. (b) Brotin, T.; Dutasta, J. P. *Chem. Rev.* **2009**, *109*, 88–130. (c) Canceill, J.; Cesario, M.; Collet, A.; Guilhem, J.; Lacombe, L.; Lozach, B.; Pascard, C. *Angew. Chem., Int. Ed. Engl.* **1989**, *28*, 1246–1248. (d) Garel, L.; Dutasta, J. P.; Collet, A. *Angew. Chem., Int. Ed. Engl.* **1993**, *32*, 1169–1171. (e) Bartik, K.; Luhmer, M.; Dutasta, J. P.; Collet, A.; Reisse, J. *J. Am. Chem. Soc.* **1998**, *120*, 784–791. (f) Luhmer, M.; Goodson, B. M.; Song, Y.-Q.; Laws, D. D.; Kaiser, L.; Cyrier, M. C.; Pines, A. *J. Am. Chem. Soc.* **1999**, *121*, 3502–3512. (g) Brotin, T.; Lesage, A.; Emsley, L.; Collet, A. *J. Am. Chem. Soc.* **2000**, *122*, 1171–1174. (h) Brotin, T.; Devic, T.; Lesage, A.; Emsley, L.; Collet, A. *Chem.;Eur. J.* **2001**, *7*, 1561–1573. (i) Lang, J.; Dechter, J. J.; Effemey, M.; Kowalewski, J. *J. Am. Chem. Soc.* **2001**, *123*, 7852–7858. (j) Tosner, Z.; Lang, J.; Sandstr€om, D.; Petrov, O.; Kowalewski, J. *J. Phys. Chem. A* **2002**, *106*, 8870–8875. (k) Brotin, T.; Dutasta, J. P. *Eur. J. Org. Chem.* **2003**, 973–984. (l) Huber, J. G.; Dubois, L.; Desvaux, H.; Dutasta, J. P.; Brotin, T.; Berthault, P. *J. Phys. Chem. A* **2004**, *108*, 9608–9615. (m) Huber, J. G.; Brotin, T.; Dubois, L.; Desvaux, H.; Dutasta, J. P.; Berthault, P. *J. Am. Chem. Soc.* **2006**, *128*, 6239–6246. (n) Fogarty, H. A.; Berthault, P.; Brotin, T.; Huber, G.; Desvaux, H.; Dutasta, J.-P. *J. Am. Chem. Soc.* **2007**, *129*, 10332–10333. (o) Zhang, C.; Shen, W.; Wen, G.; Chao, J.; Qin, L.; Shuang, S.; Dong, C.; Choi, M. M. F. *Talanta* **2008**, *76*, 235–240.

(4) Brotin, T.; Barbe, R.; Darzac, M.; Dutasta, J. P. *Chem.—Eur. J.* **2003**, *9*, 5784–5792.

(5) "Empty" means that cryptophane is not complexed by a guest molecule but it is clear that water molecules (solvent) are reversibly exchanging with the cryptophane cavity (sometimes occupied, sometimes not). Moreover, we cannot exclude the presence of dissolved gas (O_2, N_2, etc.) inside the cryptophane cavities because no vacuum treatment has been performed.

SCHEME 2. Synthesis of Cryptophanes *rac*-1, *MM*-1, and *PP*-1

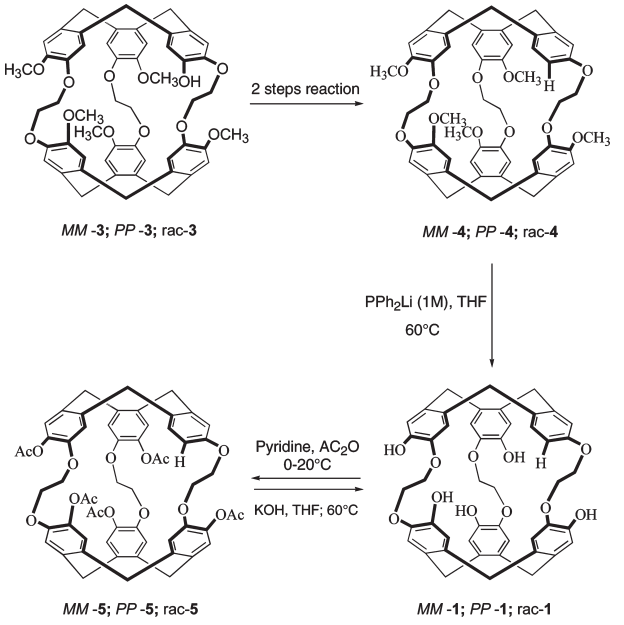

TABLE 1. Optical Rotations $[\alpha]_\lambda^{25}$ (10^{-1} deg cm^2 g^{-1}) of *MM*-5 and *PP*-5 in CH_2Cl_2, $CHCl_3$, and DMF at 25°C (Experimental Errors are Estimated to ±5%)

compd	solvent	conc.[a]	$[\alpha]_{589}^{25}$	$[\alpha]_{577}^{25}$	$[\alpha]_{546}^{25}$	$[\alpha]_{436}^{25}$	$[\alpha]_{365}^{25}$
MM-**5**	CH_2Cl_2	0.26	+10.9	+11.8	+14.3	+38.8	+119.8
PP-**5**	CH_2Cl_2	0.17	−10.2	−11.0	−15.3	−38.4	−120.7
MM-**5**	$CHCl_3$	0.15	+20.9	+21.2	+26.9	+61.7	+160.8
PP-**5**	$CHCl_3$	0.16	−19.8	−22.6	−28.2	−64.3	−165.1
MM-**5**	DMF	0.18	+4.3	+2.7	+5.8	+21.7	+79.0
PP-**5**	DMF	0.18	−3.9	−4.4	−6.0	−18.6	−74.2

[a]Concentration is given in grams per 100 mL.

for the assignment of descriptors of cryptophane molecules,[6] the *MM*-**1** derivative gives rise to the *PP*-**5** derivative. In turn, the cryptophane *PP*-**1** gives rise to the *MM*-**5** derivative. Hydrolysis of *rac*-**5**, *MM*-**5** and *PP*-**5** in a mixture of THF and KOH (1M) followed by acidification with conc. HCl provides *rac*-**1**, *MM*-**1** and *PP*-**1** derivatives in 91%, 76% and 82% yields, respectively. New cryptophanes **1** and **5** have been fully characterized by high resolution mass spectroscopy (HRMS), ^{1}H and ^{13}C NMR spectroscopy (see Supporting Information, Figures S1−S4).

Polarimetric Measurements. Polarimetric measurements of new cryptophanes **5** and **1** have been measured in various solvents and are reported in Table 1 and Table 2, respectively. Compound **5** shows in organic solvents very weak optical rotation with respect to enantiopure cryptophane-A congeners whose optical rotations have been previously measured.[1a,4] The values measured for compound *PP*-**5** are consistent with those previously obtained by Collet and co-workers for its hexa-substituted congener ($[\alpha]_{589}^{25} = -24$; $c = 0.24$; $CHCl_3$).[7]

Compound **1** shows in organic solvents (DMF, DMSO) higher optical rotation values than those measured in water

TABLE 2. Optical Rotations $[\alpha]_\lambda^{25}$ (10^{-1} deg cm^2 g^{-1}) of *MM*-1 and *PP*-1 in DMF, DMSO, and Water at 25°C (Experimental Errors are Estimated to ±5%)

compd	solvent	conc.[a]	$[\alpha]_{589}^{25}$	$[\alpha]_{577}^{25}$	$[\alpha]_{546}^{25}$	$[\alpha]_{436}^{25}$
MM-**1**	DMF	0.22	−144.6	−152.5	−176.4	−329.1
PP-**1**	DMF	0.23	+146.9	++155.4	+178.9	+345.6
MM-**1**	DMSO	0.11	−52.5	−54.2	−62.2	−128.2
PP-**1**	DMSO	0.13	+55.8	+58.9	+67.0	+133.0
MM-**1**	D_2O/NaOH	0.12	+35.7	+36.5	+42.9	+78.3
PP-**1**	D_2O/NaOH	0.11	−37.1	−40.6	−46.4	−74.2
PP-**1** + CH_2Cl_2	D_2O/NaOH	0.12	+22.9	+23.9	+22.9	+72.1
PP-**1** + $CHCl_3$	D_2O/NaOH	0.13	+64.1	+65.3	+76.7	+168.9
PP-**1**	D_2O/LiOH	0.11	−27.0	−31.4	−35.2	−57.7
PP-**1** + CH_2Cl_2	D_2O/LiOH	0.11	+28.8	+31.0	+32.6	+73.4
PP-**1** + $CHCl_3$	D_2O/LiOH	0.11	+69.6	+69.1	+77.4	+168.0
PP-**1**	D_2O/KOH	0.10	+60.6	+64.8	+78.5	+197.6
PP-**1** + CH_2Cl_2	D_2O/KOH	0.12	+40.3	+40.7	+47.1	+132.5
PP-**1** + $CHCl_3$	D_2O/KOH	0.12	+57.8	+63.9	+75.8	+194.7
PP-**1**	D_2O/CsOH	0.13	+39.1	+42.5	+52.3	+152.4
PP-**1** + CH_2Cl_2	D_2O/CsOH	0.13	+42.0	+44.4	+51.8	+148.9
PP-**1** + $CHCl_3$	D_2O/CsOH	0.14	+40.8	+45.3	+53.7	+148.6

[a]Concentration is given in grams per 100 mL.

under basic conditions and the two enantiomers *MM*-**1** and *PP*-**1** present similar optical rotation values with opposite sign. As previously observed for compound **2**,[1d] a decrease of the rotatory power is found in aqueous solutions of LiOH, NaOH and CsOH (at an arbitrary concentration of 0.1 M). In addition, the magnitude and the sign of the measured rotatory power are strongly dependent on the experimental conditions (nature of the cations and presence or not of a guest molecule inside the cavity of the cryptophane). Indeed, the empty cryptophane *PP*-**1** exhibits negative optical rotation values in LiOH ($[\alpha]_{589}^{25} = -27.0$) and NaOH ($[\alpha]_{589}^{25} = -37.1$) solutions whereas positive values have been measured in KOH ($[\alpha]_{589}^{25} = +60.6$) and CsOH ($[\alpha]_{589}^{25} = +39.1$) solutions. This feature was previously observed for compound **2** under the same experimental conditions but with a lesser extent. As a consequence, the sign of the optical rotation values cannot be used to ascertain the absolute configuration of this water-soluble cryptophane derivative. Moreover, we found that guest encapsulation modifies the sign and the magnitude of the optical rotation values in LiOH and NaOH solutions. The increase in magnitude of the rotatory power is related to the increase of the guest size (CH_2Cl_2, $CHCl_3$). On the other hand, for KOH and CsOH solutions, no significant change of the optical rotation values was observed in presence of CH_2Cl_2 and $CHCl_3$ molecules. Nevertheless, in KOH solutions, a small decrease of the rotatory power is observed in presence of CH_2Cl_2 molecules.

UV−Vis and ECD Measurements. The UV−vis spectra of empty *rac*-**1** and *rac*-**1** in presence of CH_2Cl_2 and $CHCl_3$, recorded at 20 °C under basic conditions using LiOH, NaOH, KOH and CsOH solutions at an arbitrary concentration of 0.1 M, are reported in the Supporting Information (Figure S5) in the 220−360 nm spectral range. The UV−vis spectra exhibit a strong absorption band below 220 nm corresponding to the allowed ^1B_b transition (Platt's notation) of the benzene rings and two absorption bands of medium intensity around 240 and 300 nm corresponding to the two forbidden ^1L_a and ^1L_b transitions of the benzene rings, respectively.

The ECD spectra of *MM*-**1** and *PP*-**1** have been measured under several experimental conditions by varying the pH conditions, the nature of the guest molecules and the nature

(6) IUPAC 1968 Tentative Rules, Section E, Fundamental Stereochemistry in *J. Org. Chem.* **1970**, *35*, 2849-2867. See also Collet, A.; Gabard, G.; Jacques, J.; Césario, M.; Guilhem, J.; Pascard, C. *J. Chem. Soc. Perkin. Trans. 1* **1981**, 1630–1638.

(7) Canceill, J.; Collet, A.; Gottarelli, G.; Palmieri, P. *J. Am. Chem. Soc.* **1987**, *109*, 6454–6464.

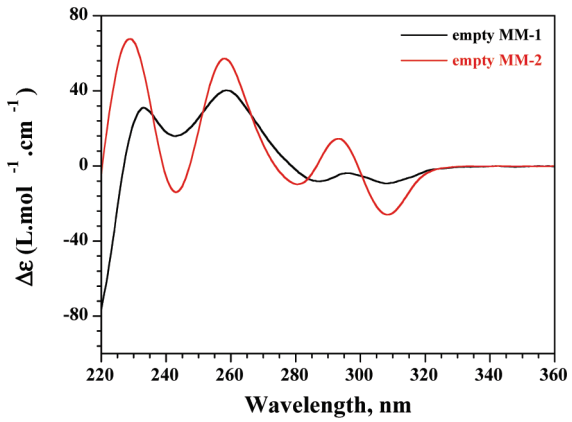

FIGURE 1. ECD spectra of *MM*-**1** and *MM*-**2** in H_2O using NaOH solution (0.1 M). The concentration of *MM*-**1** and *MM*-**2** were taken in the range $5.10^{-5}-10^{-4}$ M and the path length of the quartz cell was 0.2 cm.

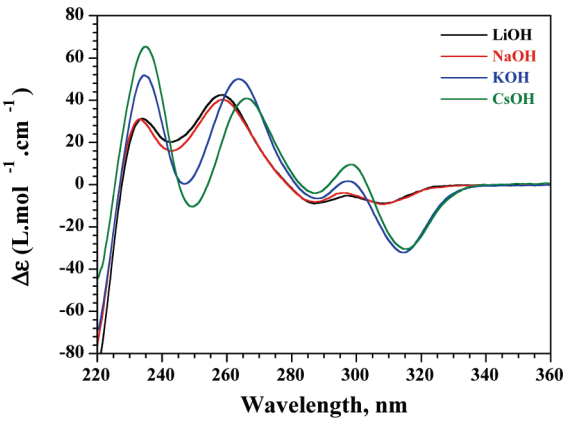

FIGURE 2. ECD spectra of *MM*-**1** in H_2O using LiOH, NaOH, KOH and CsOH solutions (0.1 M). The concentration of *MM*-**1** was taken in the range $5.10^{-5}-10^{-4}$ M and the path length of the quartz cell was 0.2 cm.

of the counterions surrounding cryptophane **1**. The ECD spectra of *MM*-**1** and *PP*-**1** exhibit perfect mirror image but for clarity only one enantiomer is shown in the following Figures 1−3. First of all, breaking the symmetry of the host considerably affects the ECD spectrum with respect to that observed for the highly symmetrical cryptophane **2**. Indeed, a comparison of the ECD spectra of compounds **1** and **2** in NaOH solution (0.1 M) reveals strong differences. For instance, in the ^1L_b region (280−330 nm), the ECD spectrum of *MM*-**1** shows two negative CD bands at 286 nm ($\Delta\varepsilon = -7.6$) and 308 nm ($\Delta\varepsilon = -8.8$). In contrast, two negative and one positive bands were previously observed in the same region for cryptophane **2**. Spectral modifications are also observed in the ^1L_a region (230−280 nm) between the two cryptophanes. These differences come from the symmetry breaking of host **1** that strongly affects the excitonic coupling (in the Kuhn-Kirkwood dipole approximation) between the six oscillators (benzene transitions). Indeed, as reported by Canceill et al.,[7] the Cotton bands of each ^1L_a and ^1L_b transitions of crytophanes having D_3-symmetry could be interpreted as the sum of three components (one A_2 component and two degenerate E components parallel and perpendicular to the C_3 axis of the cyclotriveratrylene units, respectively). The relative intensities of these components with respect to each other determine the sign and the global shape of the Cotton bands observed in the ECD spectra of highly symmetrical cryptophanes. The lack of symmetry of compound **1** (C_1-symmetry) leads to a situation where each set of Cotton bands observed for the ^1L_a, ^1L_b and ^1B_b transitions should be the result of six nondegenerated components each having different intensities and polarizations.

The ECD spectra of empty *MM*-**1** recorded under basic conditions by using aqueous solutions of LiOH, NaOH, KOH, and CsOH at an arbitrary concentration of 0.1 M are reported in Figure 2 and are found very sensitive to the nature of the counterions. These ECD spectra reveal two distinct behaviors. Similar ECD spectra are observed for LiOH and NaOH solutions, whereas they are quite different in KOH or CsOH solutions. These two last spectra exhibit Cotton bands very similar in shape and intensity to those previously observed for compound **2**.[1d]

A change of the pH conditions considerably modifies the ECD spectra of **1** (see Supporting Information, Figure S6), especially in the ^1L_b region (280−330 nm) and in the ^1B_b region ($\lambda < 230$ nm) where a strong enhancement of the Cotton band is observed with an increase of the pH. As previously mentioned for compound **2**, this effect can be associated with a conformational change of the bridges upon increasing the ionic strength of the solution. On the other hand, the ECD spectrum of **1** is also different when the hydroxyl groups are not ionized, as it is the case when experiments were performed in methanol (see Supporting Information, Figure S7).

The ECD spectra of **1** can be also strongly affected by the presence of a guest molecule inside the cavity of the host depending on the cations used. As shown in Figure 3a and b, huge modifications of the ECD spectrum of empty *MM*-**1** are observed in LiOH and NaOH solutions, when molecules such as CH_2Cl_2 (van der Waals volume, $V_{vdw} = 56.3$ Å^3)[8] or $CHCl_3$ ($V_{vdw} = 72.2$ Å^3)[8] enter the cavity of **1** (the volume of the cryptophane-A cavity with its three spacer bridges in *trans* conformations can be estimated at 95 Å^3). For instance, in the ^1L_b region, the intensity of the ECD band at 287 nm increases upon encapsulation whereas that of the band at 310 nm vanishes. ECD changes are more pronounced at shorter wavelength in the ^1B_b region. Indeed, a strong enhancement of the ECD band at 220 nm is observed, going from $\Delta\varepsilon = -82$ for the empty *MM*-**1** to $\Delta\varepsilon = -180$ for the $CHCl_3$@*MM*-**1** complex.[9] In contrast, the ECD band in the ^1L_a region (240−280 nm) appears less affected by the encapsulation process. The encapsulation process or an increase of the pH induces the same modifications of the ECD spectra in LiOH and NaOH solutions.

We have found that guests having a smaller van der Waals volume such as CH_3Cl ($V_{vdw} = 42$ Å^3) or xenon ($V_{vdw} = 42$ Å^3) do not significantly modify the ECD spectrum of **1** in NaOH solutions (see Supporting Information, Figure S8) and, in particular, the ECD band at 220 nm is not affected by the encapsulation process. The small occupancy factor

(8) Zhao, Y. H.; Abraham, M. H.; Zissimos, A. M. *J. Org. Chem.* **2003**, *68*, 7368–7373.

(9) The experimental conditions (concentration of cryptophane and path length of the quartz cell) have been optimized to obtain the best signal-to-noise ratio over the largest spectral range. These experimental conditions prevent experiments below 220 nm due to detector saturation.

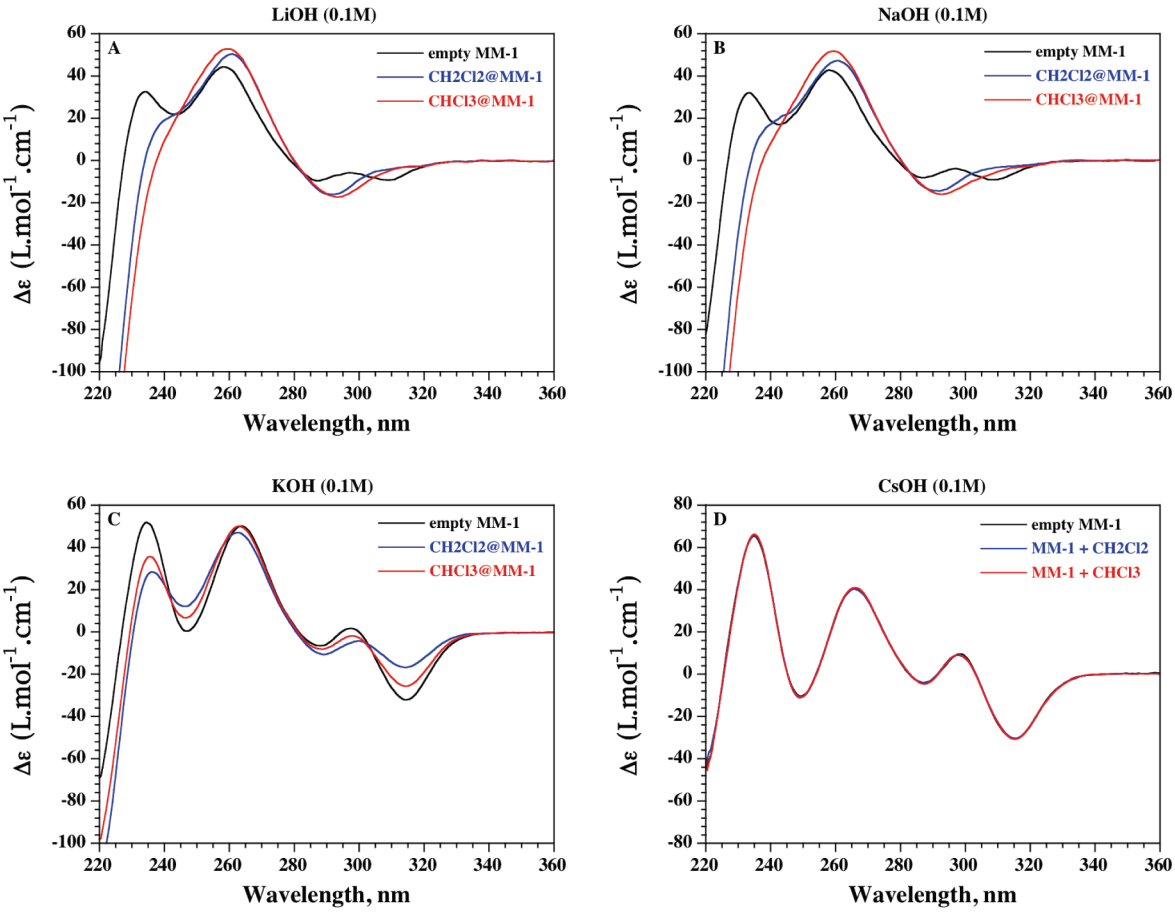

FIGURE 3. ECD spectra of empty *MM*-**1** as well as *MM*-**1** in presence of CH_2Cl_2 and $CHCl_3$ in H_2O; aqueous solutions of (A) LiOH, (B) NaOH, (C) KOH, and (D) CsOH were used. The concentration of *MM*-**1** was taken in the range $5.10^{-5}-10^{-4}$ M and the path length of the quartz cell was 0.2 cm.

(40−45%) of these guest molecules inside the cavity of host **1** is probably responsible for this feature. In contrast, guest molecules having a larger van der Waals volume, such as CH_3I (V_{vdw} = 54.6 Å^3), CH_2BrCl (V_{vdw} = 60.4 Å^3), CH_2Br_2 (V_{vdw} = 64.4 Å^3), and CH_2ClI (V_{vdw} = 66.4 Å^3) significantly modify the ECD spectrum of **1** and the ECD spectra of these complexes differ from each other (see Supporting Information, Figure S9). The encapsulation process is clearly visible in ^1L_b region (the only region of the spectrum accessible with all these guests), and results in an increase of the ECD band at 295 nm and a decrease of the ECD band observed at 310 nm for the empty host **1**. Larger molecule such as CH_2I_2 (V_{vdw} = 76.5 Å^3) unable to enter the cavity of **1** leaves the ECD spectrum unchanged (spectrum not shown). Similar results have been obtained when lithium cation was used as a counterion (see Supporting Information, Figures S10−S11).

In KOH solution, spectral modifications are observed for *MM*-**1** in presence of CH_2Cl_2 and $CHCl_3$ in the ^1B_b and ^1L_b regions (see Figure 3c). Surprisingly, these spectral modifications are more pronounced for the CH_2Cl_2@*MM*-**1** complex. The ECD spectrum of $CHCl_3$@*MM*-**1** complex shows an intermediate behavior. This result distinguishes from that previously observed for compound **2** in the same experimental conditions.[1d] Finally, in CsOH solution, the ECD spectra of empty *MM*-**1** and *MM*-**1** in presence of CH_2Cl_2 and $CHCl_3$ remain unchanged (see Figure 3d) and no encapsulation effect is observed.

IR and VCD Measurements. IR and VCD measurements of **1** have been performed in deuterated aqueous solutions of NaOD, KOD and CsOD. Samples of **1** have been prepared with a concentration of 0.03 M to provide VCD spectra with a sufficient signal-to-noise ratio. IR absorption spectra of *rac*-**1** have been recorded under various basic conditions using solutions of NaOD, KOD and CsOD in D_2O at different concentrations from 0.056 M (pD = 13.6) to 0.592 M (pD = 14.6). The results obtained using solutions of NaOD in D_2O are reported in Figure 4a in the 1650−1350 cm^{-1} spectral range, for which the changes are the most noteworthy. The isosbestic point located at 1505 cm^{-1} reveals the coexistence of two distinct forms of the hydroxyl groups in the solution. As previously shown for hexa-hydroxyl cryptophane, these two components of the ν_{19a}C=C stretching vibration of the rings are associated with the protonated (phenol) and deprotonated (phenolate) species.[1d] This result has been confirmed by the calculated absorption spectra reported in Figure 4b. DFT calculations of the absorption spectra have been carried out for the phenol and phenolate forms of empty *PP*-**1**. The high-frequency component at 1507 cm^{-1} is characteristic of the phenol form whereas the low-frequency component at 1493 cm^{-1} is characteristic of the phenolate form of the cryptophane **1**. The averaged spectrum 1OD+4ONa reproduces fairly well the experimental spectrum recorded for 0.21 M sodium concentration. This result shows that a higher proportion

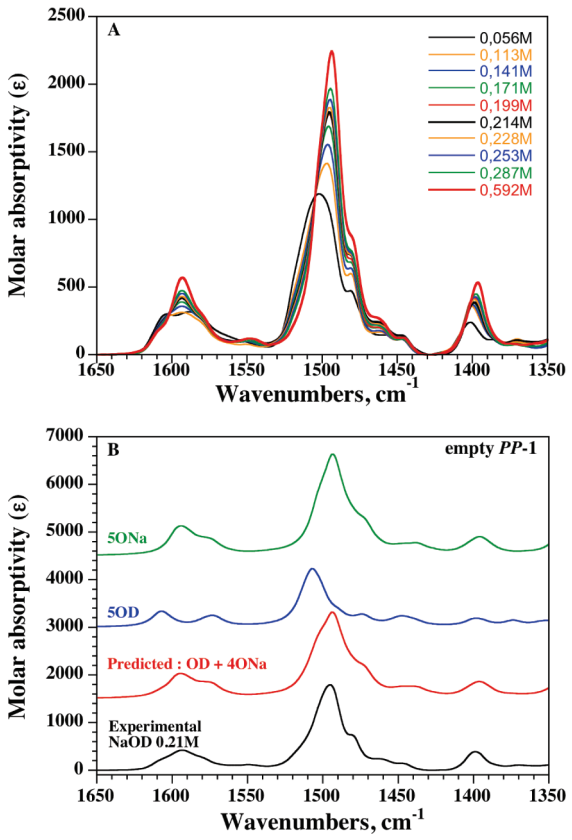

FIGURE 4. (A) IR spectra of *rac*-**1** in D_2O using NaOD solutions at different concentrations. The concentration of host **1** was 0.030 M. (B) Comparison of experimental IR spectrum of empty *PP*-**1** in D_2O using NaOD solution (0.21 M) with calculated spectra at the B3PW91/6-31G* levels of the phenol (5OD) and phenolate (5ONa) forms of *PP*-**1**.

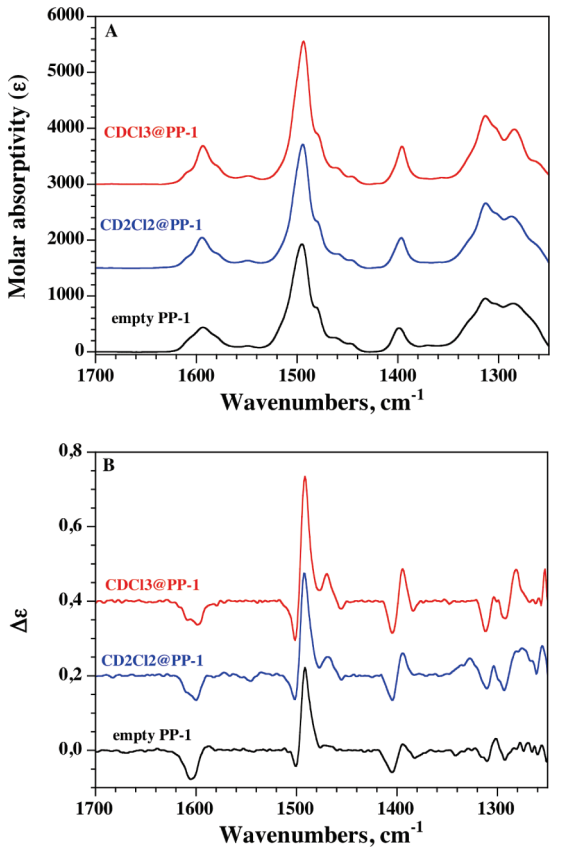

FIGURE 5. (A) IR and (B) VCD spectra of empty *PP*-**1** as well as CD_2Cl_2@*PP*-**1** and $CDCl_3$@*PP*-**1** complexes in D_2O using NaOD solution (0.21 M). The concentration of host **1** was 0.030 M.

(80%) of phenolate groups occurs in compound **1** at this sodium concentration with respect to the 50% found for compound **2**. For a highest sodium concentration (i.e., 0.59 M), all the hydroxyl groups are deprotonated.

Other absorption bands are affected by the concentration of NaOD. For instance, the band located around 1400 cm^{-1}, which corresponds to a coupled mode involving wagging and twisting vibrations of the CH_2 groups (linkers), increases when the pD is raising in the solution. In the same way, the band associated with the $\nu_{8a}C{=}C$ stretching vibration of the rings, around 1590 cm^{-1}, undergoes large modifications when the pD is changed. At low concentrations of NaOD, this band is composed by two distinct components located at 1603 and 1589 cm^{-1}. These two components are well reproduced by the calculated spectrum of the penta-phenol form. When the pD of the solution is increasing, the two previous components give rise to an unique band growing at 1593 cm^{-1}. The intensity of this band becomes much higher. All these spectral modifications are well reproduced by the calculated absorption spectrum of the phenolate form of *PP*-**1**. The same behavior occurred when NaOD solution was replaced by KOD and CsOD solutions (see Supporting Information, Figures S12−S13).

The IR and VCD spectra of empty and complexed *PP*-**1** are reported in Figure 5a and b, respectively. The experiments have been performed in D_2O using NaOD solution at a concentration of 0.21M. The spectra have been recorded in presence of CD_2Cl_2 and $CDCl_3$, and are presented in the 1700−1250 cm^{-1} region. A slight enhancement of the IR and VCD bands is observed on the experimental spectra of the complexed *PP*-**1**. It is noteworthy that the same spectral changes occur in the IR and VCD spectra of empty *PP*-**1** when a higher concentration in sodium (0.59 M) is used. These spectral modifications have already been observed for compound **2**, to a larger extent, and have been explained using theoretical calculations by a conformational change of the linkers upon encapsulation.

The same study has also been performed with solutions of deuterated potassium and cesium hydroxide in D_2O at a concentration of 0.21 M. The IR and VCD spectra do not change when CD_2Cl_2 or $CDCl_3$ molecules were added to the KOD and CsOD solutions (see Supporting Information, Figures S14−S15).

Discussion

Conformational Analysis of 1. The average conformation of host **1** and its eventual modification upon encapsulation of guests have been determined from molecular mechanics (MM) and molecular dynamics (MD) calculations. These calculations were performed for the phenol and phenolate forms with Na^+ as counterions of empty *PP*-**1** (Figure 6) and $CHCl_3$@*PP*-**1** complex (Figure 7), with three different conformations of -OCH_2CH_2O- linkers as initial conditions: *all-trans* conformation where the three dihedral angles are 180°

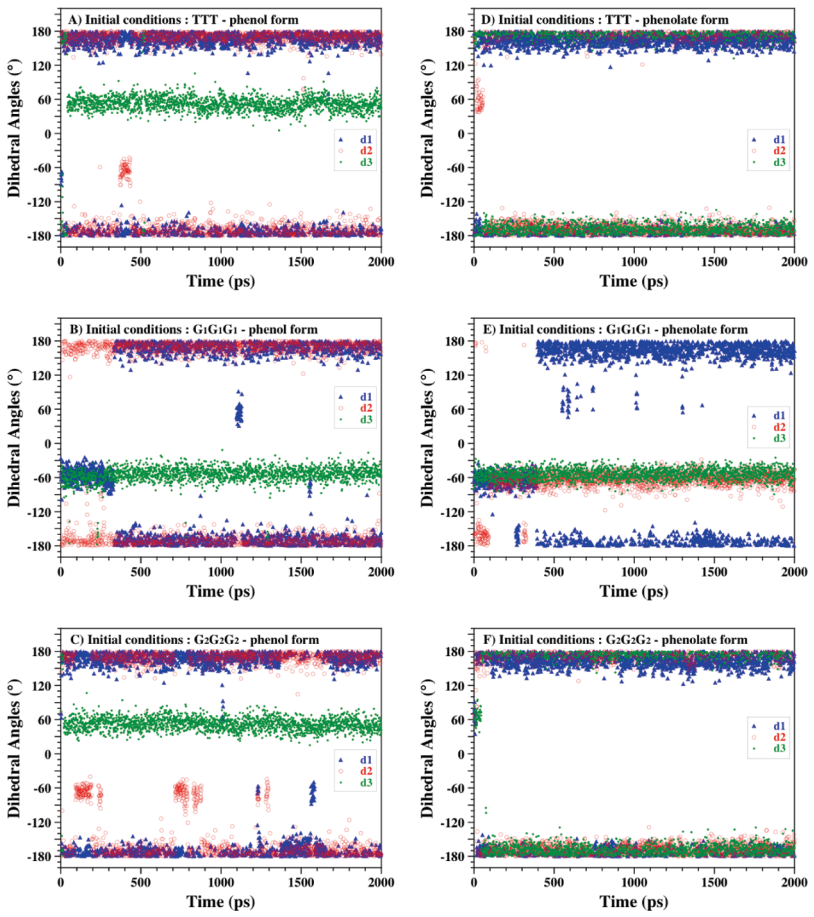

FIGURE 6. Dihedral angles of the three linkers during the 2 ns of the dynamics. These values have been extracted from the MD calculations for the phenol (A, B, and C) and phenolate (E, F, and G) forms of empty *PP*-**1** starting from the *TTT* (A and D), $G_1G_1G_1$ (B and F), and $G_2G_2G_2$ (C and F) conformations of the linkers.

(labeled *TTT*) and *all-gauche* conformations where the three dihedral angles are −60° (labeled $G_1G_1G_1$) or +60° (labeled $G_2G_2G_2$). It is noteworthy that the three linkers do not have the same chemical environment. Indeed, the two first linkers (noted d_1 and d_2) are surrounded by two hydroxyl groups, while the last one (d_3) is surrounded only by one hydroxyl group.

As shown in Figure 6, after few steps of dynamics, the starting *TTT*, $G_1G_1G_1$, and $G_2G_2G_2$ conformations of the linkers are left. Two conformations clearly appear for the phenol form of empty *PP*-**1**: the first one with the two dihedral angles d_1 and d_2 around ±180°, and d_3 around −60°; the second conformation, with angles d_1 and d_2 around ±180°, and d_3 around +60°. Therefore, the phenol form of empty *PP*-**1** favors the *TTG* conformation of the linkers. It is interesting to note that the *gauche* conformation occurs for the linker d_3, that is surrounded only by one hydroxyl group. When MD computations are performed in presence of Na^+ cations (phenolate form), the results are quite different from those obtained for the cryptophane with hydroxyl groups. Indeed, the *all-trans* conformation of the linkers with the three dihedral angles d_1, d_2, and d_3 around ±180° is favored. We have also observed that some Na^+ cations are in the vicinity of the portals of *PP*-**1** (see Supporting Information, Figures S17). Indeed, two sodium cations are localized in the two portals exhibiting the smaller windows, at an average distance of 3.5 Å from the center of the cryptophane cavity. These two cations interact not only with the O^-, but also with the oxygen of the linker, which may modify its conformation. Finally, MD calculations performed for the $CHCl_3$@*PP*-**1** complex (see Figure 7) reveal that the *TTG* conformation of the linkers is again the most favorable, even though the *TTT* conformation may occur in presence of Na^+ cations.

To confirm the MD results and to evaluate the energy differences between the possible conformations of the linkers, DFT calculations of the IR spectra of empty *PP*-**1** and $CDCl_3$@*PP*-**1** complex have been achieved for both the phenol and phenolate forms of the molecule. For each form, the geometries were optimized at the B3PW91/6-31G* level for the *TTT*, $G_1G_1G_1$, $G_2G_2G_2$, and TTG_1 conformations of the three linkers. Harmonic vibrational frequencies were calculated at the same level to show that all structures are stable conformations and to enable free energies to be calculated. The optimized Gibbs energies and the O−C−C-O dihedral angles of the three linkers are listed in Table 3. The optimized geometries calculated for the phenol and phenolate forms of empty *PP*-**1** show that the *TTG* conformation of the linkers leads to the lowest Gibbs free energy. Indeed, the *all-trans* and *all-gauche* conformations are more than 3 kcal/mol higher in free energy. For $CDCl_3$@*PP*-**1** complex, the optimized geometries calculated for the *TTT* and *TTG* conformations lead to very close Gibbs free energies for both phenol and phenolate forms. The addition

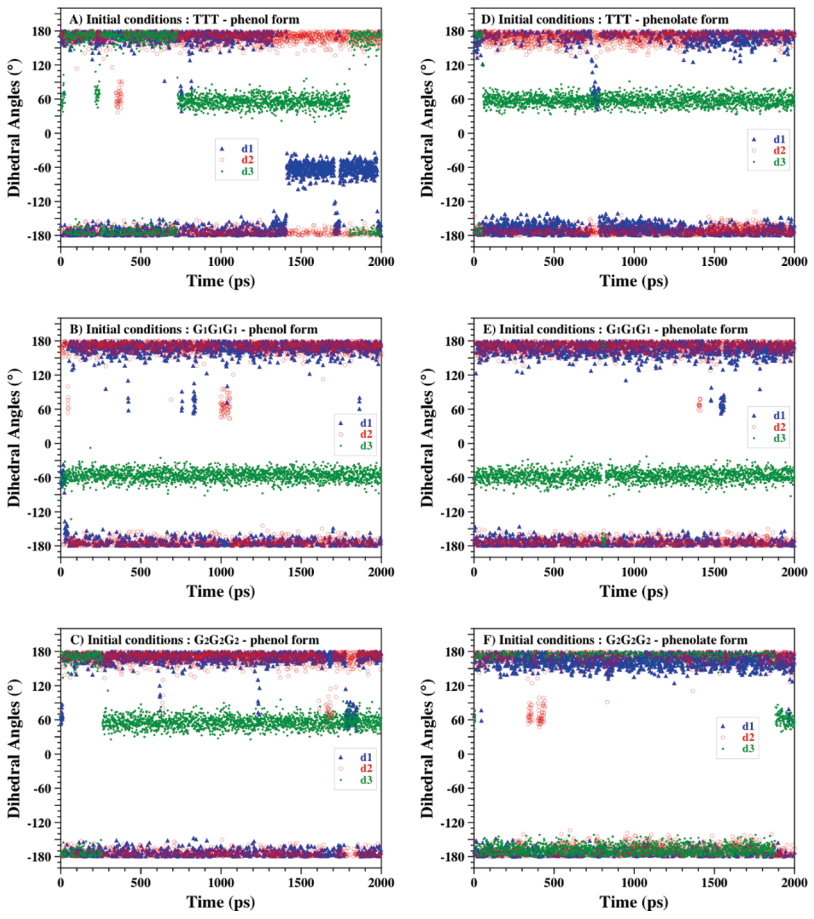

FIGURE 7. Dihedral angles of the three linkers during the 2 ns of the dynamics. These values have been extracted from the MD calculations for the phenol (A, B, and C) and phenolate (E, F, and G) forms of $CHCl_3$@*PP*-**1** complex starting from the *TTT* (A and D), $G_1G_1G_1$ (B and F), and $G_2G_2G_2$ (C and F) conformations of the linkers.

TABLE 3. Conformations and Energies of *PP*-1

form	conformer	Gibbs energy (hartrees)	ΔE (kcal.mol^{-1})	$d_1{}^a$ (deg)	$d_2{}^a$ (deg)	$d_3{}^a$ (deg)
			empty *PP*-**1**			
Phenol	*TTT*	−2680.051655	8.4	−163.5	−166.3	−170.3
	$G_2G_2G_2$	−2680.053873	7.1	66.7	69.2	69.4
	$G_1G_1G_1$	−2680.058339	4.3	−58.2	−56.0	−64.2
	TTG_1	−2680.065149	0.0	−168.5	−168.8	−60.5
Phenolate	$G_1G_1G_1$	−3488.690295	5.4	−57.9	−84.1	−53.2
	TTT	−3488.693834	3.2	168.7	−94.0	−151.4
	$G_2G_2G_2$	−3488.693931	3.1	54.9	59.6	69.8
	TTG_1	−3488.698931	0.0	−171.7	−83.5	−52.1
			$CDCl_3$@*PP*-**1**			
Phenol	$G_2G_2G_2$	−4099.124176	18.4	89.6	90.5	87.2
	$G_1G_1G_1$	−4099.143013	6.6	−70.0	−70.3	−67.4
	TTT	−4099.152698	0.5	175.5	178.5	179.8
	TTG_1	−4099.153548	0.0	175.7	173.7	−64.5
Phenolate	$G_1G_1G_1$			no convergence		
	$G_2G_2G_2$	−4907.750966	2.8	74.1	55.9	76.1
	TTG_1	−4907.754003	0.9	−145.5	−106.3	−54.8
	TTT	−4907.755435	0.0	−169.6	−156.3	−157.5

[a]Dihedral angle O−C−C−O.

of a chloroform molecule in the cryptophanol cage stabilizes the *TTT* conformer. A similar result was previously reported for cryptophane-A monofunctionalized with a hydrogen atom.[1c] This result is not surprising due to the good size matching between the chloroform (c.a. 72.2 Å^3) and the cryptophane cavity in its *all-trans* conformation (c.a. 95 Å^3).

On the basis of the MD and DFT calculations, it can be concluded that the *TTG* conformation of the linkers is the most favorable for the empty *PP*-**1**. The presence of Na^+ cations (phenolate form) for the empty *PP*-**1** as well as the presence of chloroform in the cavity of *PP*-**1** favor the *TTT* conformation of the linkers. Thus, the relative populations

of the many different possible conformers of cryptophane is altered upon guest complexation such that, on average, the linkers preferentially adopt the *TTG* conformation in the absence of guest molecule whereas the linkers more often adopt *trans* conformations in the presence of encapsulated guests. Indeed, empty cryptophanol, which is a lipophilic molecule, even though it is soluble under basic conditions (pH ≥ 12), allows the presence of *gauche* conformations of the linkers in order to reduce the size of its internal cavity in water (hydrophobic effect). In contrast, encapsulation of a guest molecule requires host **1** to change the conformation of its linkers in order to enlarge the cavity to accommodate the guest. Thus, upon encapsulation, host **1** stabilizes *trans* conformation of the linkers when large molecules are present in the cavity. Of course the stabilization of the *trans* conformations of the linkers strongly depends on the size of the guest. A large guest such as a chloroform molecule (V_{vdw} = 72.2 Å^3) is less easily accommodated in the cavity of **1** with respect to a dichloromethane guest (V_{vdw} = 56.3 Å^3) and thus it requires host **1** to significantly enlarge the size of its cavity. The preferential *all-trans* conformation of the linkers is certainly associated with the slight enhancement of the IR and VCD bands for $CDCl_3$@*PP*-**1** complex.

Encapsulation and Counterion Effects. Polarimetry as well as ECD and VCD spectroscopies clearly reveal the molecular recognition of small neutral molecules by cryptophane hosts. Indeed, the encapsulation effect is characterized for water-soluble cryptophanes by a significant increase in magnitude of the rotatory power as well as by a change of its sign in polarimetry and by large modifications in the ECD and VCD spectra. Encapsulation effect has been clearly evidenced for host **1** in LiOH and NaOH solutions, as previously observed for host **2**.[1d] This property makes these two cryptophanes excellent molecular sensors to detect small neutral molecules dissolved in water. Moreover, the size of the counterion plays a key role in the overall chiroptical properties of the host. In the case of LiOH or NaOH solutions, the size of the cations (V = 1.8 Å^3 and V = 4.4 Å^3 for Li^+ and Na^+, respectively)[10] is too small to obstruct the three windows of the host molecule, allowing guest molecules with appropriate size to enter the cavity of **1**. In addition, Li^+ and Na^+ cations do not show any affinity for the cavity of the host as demonstrated from MD calculations (see Supporting Information, Figures S17). In turn, the guest molecules, depending on their molecular volume, modify the conformation of the bridges and induce a large modification of the chiroptical properties of the host. This effect is clearly visible on both ECD and VCD spectra (see Figures 3b and 5b), where significant spectral modifications are observed. In addition, we have found that the ECD band in the ^1B_b region of the spectrum (around 220 nm) is extremely sensitive to guest encapsulation and an increase of this ECD band appears as a good probe to ascertain the binding of a guest molecule by host **1**. Thus, this result suggests that the 180−220 nm region of the ECD spectrum of cryptophane should be investigated in more detail in the future. In contrast, no encapsulation effect has been observed from chiroptical spectroscopies in CsOH solution. This feature has also been noted by NMR experiments (^{1}H NMR and ^{129}Xe-NMR) of solutions containing **2** in presence of dissolved xenon.[11] One interpretation is that the cesium cations are big enough (V = 19.5 Å^3 for Cs^+)[10] to obstruct the three windows of **1** and to prevent any guest from entering its cavity. An other interpretation is that cesium cations are encapsulated and, being present in very large excess, are occupying the cavities such that guests can not enter. This assumption may be supported by our MD calculations, showing that one cesium cation is able to enter the cavity of *PP*-**1** (see Supporting Information, Figures S18). Moreover, additional ECD experiments reveal that the spectrum recorded for *MM*-**1** in CsOH solution (0.1 M) remains unchanged when *MM*-**1** is dissolved in LiOH solution (0.1 M) with a very small amount of CsOH (2×10^{-4} M), in presence (saturated solution) or not of $CHCl_3$ guest molecule (see Supporting Information, Figures S19). The fact that the complexation of cesium is not perturbed by the presence of a large excess of chloroform molecules indicates that **1** acts as a very good complexing host molecule for cesium cations. This interesting feature makes host **1** the first cryptophane molecule showing affinity for an alkali cation in water.

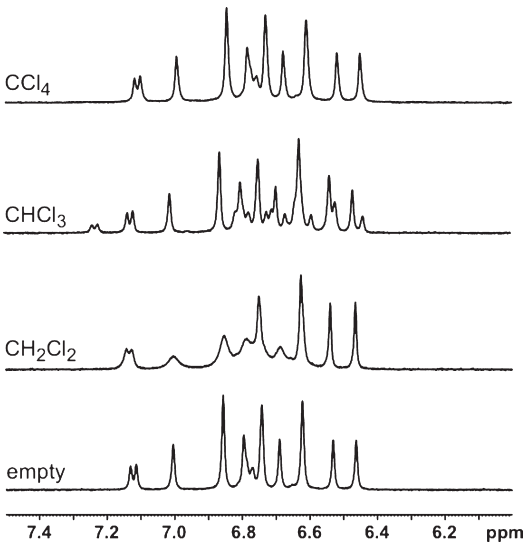

FIGURE 8. ^{1}H NMR spectra of *rac*-**1** (aromatic region) in presence of CH_2Cl_2, $CHCl_3$, and CCl_4 in D_2O/KOD solution (0.1 M) at 298 K.

An intermediate behavior occurs in KOH solution. The addition of CH_2Cl_2 or $CHCl_3$ guest molecules in the KOH solution slightly changes the ECD spectrum of **1** (see Figure 3c), indicating that CH_2Cl_2 or even $CHCl_3$ are well recognized by **1**. Moreover, the ^{1}H NMR spectrum of *rac*-**1** recorded at 298K in KOD solution reveals modifications in the aromatic region (see Figure 8), indicating an interaction between CH_2Cl_2 or $CHCl_3$ guest molecules and host **1**. Indeed, a broadening of some aromatic signals is observed in presence of CH_2Cl_2, whereas a new set of signals appears in presence of $CHCl_3$. These spectral changes (with respect to the ^{1}H NMR spectrum of empty *rac*-**1**) indicates that $CHCl_3$ is in a slow exchange regime at the NMR time scale, whereas CH_2Cl_2 is near the fast-slow exchange resolution limit.

(10) The volume of alkali metal ions have been calculated from their ionic radii.

(11) Berthault, P.; Desvaux, H.; Wendlinger, T.; Gyejacquot, M.; Stopin, A.; Brotin, T.; Dutasta, J. P.; Boulard, Y *Chem.—Eur. J.* **2010**, *16*, 12941–12946.

However, when the ^{1}H NMR spectra of *rac*-**1** were recorded at 278K, the decrease of the host−guest exchange dynamics appears sufficient to reveal the presence of the bound CH_2Cl_2 signal located at 1.1 ppm (see Supporting Information, Figure S16). This result clearly indicates that encapsulation effect occurs in KOH solution. In contrast, a larger molecule such as CCl_4 (V_{vdw} = 86.7 Å^3), too big to enter the cavity of *PP*-**1**, leaves the ^{1}H NMR spectrum of **1** unchanged.

Conclusion

The two enantiomers of a new water-soluble cryptophane **1** (penta-hydroxyl cryptophane-A) were synthesized and their chiroptical properties in water under basic conditions were examined by ECD and VCD spectroscopies depending on the pH, the nature of the counterions and the size of the guest molecules. As previously reported for a cryptophane congener bearing six hydroxyl functions, cryptophane **1** exhibits unusual chiroptical properties in basic water with respect to cryptophane derivatives soluble in organic media. The observed chiroptical changes can be interpreted by conformational changes of the bridges due to the presence of cations in the vicinity of the host or guest molecules within its cavity. These chiroptical modifications are clearly visible in the ECD spectra of **1**, especially in the ^1L_b and the ^1B_b regions. This makes host **1** a good sensor for studying molecular recognition phenomena with small neutral molecules in LiOH or NaOH solutions. In KOH solution, compound **1** exhibits a quite different behavior than host **2** under the same experimental conditions, since ECD spectra are altered by addition of CH_2Cl_2 or $CHCl_3$ into the solution. ^{1}H NMR experiments show that the CH_2Cl_2 and $CHCl_3$ guest molecules are in fast and slow exchange at the NMR time scale with host **1**, respectively. In contrast, in CsOH solution, no encapsulation effect was revealed by ECD spectroscopy whatever the guest molecule studied. This peculiar behavior comes from the fact that cesium cations are very well encapsulated inside the cavity of host **1**. This interesting feature noticed with host **1** prompts us to reinvestigate in more details the possible binding of alkali cations with host **2**. Indeed, even though our experimental results were fully consistent with steric effects induced by the K^+ and Cs^+ cations, the possible binding of these two cations by host **2** cannot be totally excluded in the light of these new results brought by MD calculations.

The presence of a single hydrogen atom replacing a hydroxyl function in one CTV bowl creates a larger window in one of the three portals of **1**. This feature allows small chiral molecules such as propylene oxide to easily enter the cavity of **1** whereas its complexation is more difficult with compound **2**. The enantioselective complexation of small chiral guests by cryptophane **1** will be studied in the near future.

Experimental section

NMR Spectroscopy and Polarimetric Measurements. ^{1}H and ^{13}C NMR spectra were recorded at 500 and 125.76 MHz, respectively, using a 5-mm liquid probe (nonspinning). Optical rotations of *MM*-**1**, *PP*-**1**, *MM*-**5** and *PP*-**5** were measured at several wavelengths on a polarimeter with a 100 mm cell thermostatted at 25 °C.

UV−Vis and ECD Measurements. UV−vis and ECD spectra were recorded at room temperature using quartz cell with path length of 0.5 and 0.2 cm, respectively. Concentration of *MM*-**1** and *PP*-**1** was taken in the range 5.10^{-5}−10^{-4} M in basic H_2O solutions (0.1 M solutions of LiOH, NaOH, KOH, and CsOH). Saturated solutions of various halomethanes in water have been used to study encapsulation of guest molecules. Spectra were recorded in the 220−450 nm wavelength range with a 0.5 nm increment and a 1s integration time. Spectra were processed with standard spectrometer software, baseline corrected and slightly smoothed by using a third order least-squares polynomial fit. Spectral units were expressed in molar ellipticity.

IR and VCD Measurements. The infrared and VCD spectra were recorded with a FTIR spectrometer equipped with a VCD optical bench.[12] IR absorption and VCD spectra were recorded at a resolution of 4 cm^{-1}, by coadding 50 scans and 24000 scans (8 h acquisition time), respectively. Samples were held in a CaF_2 cell with a fixed path length of 45 μm. IR and VCD spectra of *MM*-**1** and *PP*-**1** were measured in basic D_2O solutions (0.21 M solutions of NaOD, KOD, and CsOD) at a concentration of 0.030 M. Additional IR spectra of *rac*-**1** were recorded for various concentrations of NaOD, KOD, and CsOD. Baseline corrections of the VCD spectra were performed by subtracting the two opposite-enantiomer VCD spectra of **1** (recorded under the same experimental conditions) with division by two. In all experiments, the photoelastic modulator was adjusted for a maximum efficiency at 1400 cm^{-1}. Calculations were done with the standard spectrometer software, using Happ and Genzel apodization, de-Haseth phase-correction and a zero-filling factor of 1. Calibration spectra were recorded using a birefringent plate (CdSe) and a second BaF_2 wire grid polarizer, following the experimental procedure previously published.[13] Finally, in the presented IR spectra, the solvent absorption was subtracted out.

MM and MD Calculations. Molecular mechanics (MM) and molecular dynamics (MD) calculations have been performed with the Tinker package[14] and the OPLS force-field[15] in a periodic box big enough to avoid self-interaction problems. We applied a cutoff for Van der Walls interaction of 10 Å. The solute has been soaked in a cubic box of solvent (size 27.936 Å) containing 729 molecules of water. Given the cutoff of 10 Å, this simulation box is large enough to avoid self-interaction between the cryptophane and its images. The process to dissolve the cryptophane in water was done by placing the molecule into the simulation box of a thermally equilibrated water at a concentration of 1 g/cm^3 and by subsequent removal of solvent molecules overlapping with the cryptophane. MD calculations have been performed in the canonical ensemble (NVT) at 300 K using the Berendsen thermostat,[16] with different values for the dihedral angle of the -OCH_2CH_2O- linker as initial conditions. The three linkers were considered either with a *trans* conformation (referring to the bonds to the O atoms having a ±180° dihedral angle, labeled *TTT*) or with a *gauche* conformation (− 60° dihedral angle, labeled $G_1G_1G_1$ or +60° dihedral angle, labeled $G_2G_2G_2$). During the 2 ns of the dynamics, the values of the dihedral angles of the linkers and the distances between the counterions and the center of the cryptophane are recorded every ps.

(12) Buffeteau, T.; Lagugné-Labarthet, F.; Sourrisseau, C. *Appl. Spectrosc.* **2005**, *59*, 732–745.

(13) Nafie, L. A.; Vidrine, D. W. In *Fourier Transform Infrared Spectroscopy*; Ferraro, J. R., Basile, L. J., Eds.; Academic Press: New York, 1982; Vol. 3, pp 83−123.

(14) Ponder, J. W. *TINKER*, Ver. 5.1; 2010; http://dasher.wustl.edu/tinker

(15) (a) Jorgensen, W. L.; Maxwell, D. S.; Tirado-Rives, J. *J. Am. Chem. Soc.* **1996**, *117*, 11225–11236. (b) Maxwell, D. S.; Tirado-Rives, J.; Jorgensen, W. L. *J. Comput. Chem.* **1995**, *16*, 984–1010. (c) Jorgensen, W. L.; McDonald, N. A. *Theochem−J. Mol. Struct.* **1998**, *424*, 145–155. (d) McDonald, N. A.; Jorgensen, W. L. *J. Phys. Chem. B* **1998**, *102*, 8049–8059. (e) Rizzo, R. C.; Jorgensen, W. L. *J. Am. Chem. Soc.* **1999**, *121*, 4827–4836. (f) Price, M. L. P.; Ostrovsky, D.; Jorgensen, W. L. *J. Comput. Chem.* **2001**, *22*, 1340–1352.

(16) Berendsen, H. J. C.; Postma, J. P. M.; van Gunsteren, W. F.; DiNola, A.; Haak, J. R. *J. Chem. Phys.* **1984**, *81*, 3684–3690.

DFT Calculations. The geometry optimizations, vibrational frequencies and absorption intensities were calculated by Gaussian 03 program[17] on sixteen processors at the M3PEC computing center of the University Bordeaux I. Calculations of the optimized geometry of empty *PP*-**1** and $CDCl_3$@*PP*-**1** complex were performed at the density functional theory level using B3PW91 functional and 6-31G* basis set. The theoretical framework for geometry optimization of cryptophane molecules has been previously published.[1a] Since experiments were performed in basic solutions leading to partially deprotonated cryptophanol, DFT calculations were performed considering the phenol (OH peripheral substituents) and phenolate (O^- Na^+ peripheral substituents) forms of the molecule with the *TTT*, $G_1G_1G_1$, $G_2G_2G_2$ and G_1TT conformations of the three -OCH_2CH_2O- bridges. Vibrational frequencies and IR intensities were calculated at the same level of theory. For comparison to experiment, the calculated frequencies were scaled by 0.957 and the calculated intensities were converted to Lorentzian bands with a half-width of 7 cm^{-1}.

Synthesis of *rac*-5, *MM*-5 and *PP*-5 from Cryptophanes 4. A solution of freshly prepared PPh_2Li (1M, 5.4 mL, 5.4 mM) was added dropwise via syringe to a stirred solution of *rac*-**4** (0.3 g, 0.35 mM) in THF (3 mL) under an argon atmosphere and at room temperature. After complete addition the dark red solution was heated at 60 °C for 16 h. The mixture was poured in water (40 mL) and extracted four times with CH_2Cl_2. Acidification of the aqueous layer with conc. HCl gives rise to a white precipitate, which was collected on a frit and washed with water, dried and then washed with diethyl ether. The solid residue was purified on a silica gel column chromatography (L = 20 cm, Acetone/DMF: 50/50). The yellow-orange fractions were collected and the solvents were removed by rotary evaporation. Diethyl ether was added to the oily residue and the mixture was stirred overnight to give a beige powder, which was collected on a frit. The solid (0.19 g) was dissolved at 0 °C in dry pyridine (5 mL) and anhydride acetic (1.4 mL) was added dropwise. After complete addition the orange solution was allowed to warm to room temperature and stirred for an additional 2−3 h. The solution was then poured in a mixture of CH_2Cl_2 and water. The organic layer was washed twice with water and dried over sodium sulfate. After filtration the solvent was removed by rotary evaporation and the residue was purified by column chromatography (CH_2Cl_2/Acetone: 90/10). The product was recrystallized in a $CHCl_3$/EtOH mixture. The crystals were collected on a frit and washed with diethyl ether to give *rac*-**5** (0.17 g, 51% yield from *rac*-**4**). Using the same synthetic route the enantiopure derivatives *MM*-**5** (55% yield) and *PP*-**5** (60% yield) have been obtained from *PP*-**4** and *MM*-**4**, respectively. Mp (DSC) > 300 °C. ^{1}H NMR (500 MHz, CD_2Cl_2, 25 °C) δ 7.14 (d, 1H, ^3J(H,H) = 8.4 Hz; Ar), 6.94 (s, 1H; Ar), 6.91 (s, 3H; Ar), 6.90 (s, 1H; Ar), 6.89 (s, 1H; Ar), 6.83 (s, 2H; Ar), 6.80 (s, 1H; Ar), 6.70 (s, broad, 1H; Ar), 6.69 (s, 1H; Ar), 6.54 (d, 1H, ^3J(H,H) = 8.4 Hz; Ar), 4.47−4.56 (6d; H_a), 4.40−3.85 (m, 12H; CH_2), 3.55−3.45 (6d; H_e), 2.40 (s, 3H; CH_3), 2.35 (s, 3H; CH_3), 2.32 (s, 6H; 2*CH_3), 2.31 (s, 3H; CH_3). ^{13}C NMR (125.76 MHz, CD_2Cl_2, 25 °C) δ 169.3, 169.2 (2C), 169.1, 169.0, 156.9, 149.5, 149.3, 149.2, 149.0, 148.2, 141.2 (2C), 141.1, 140.7, 140.3, 139.9, 138.9, 138.4, 138,1, 137.6 (2C), 135.0, 134,3, 134.1, 133.8, 132.0, 131.4, 131.3, 124.9 (3C), 124.8, 124.1, 122.0, 121.7, 120.1 (2C), 119.1, 116.3, 111.5, 70.2, 70.0, 69.6, 69.0, 66.5, 64.6, 36.5, 36.4 (2C), 36.3, 36.2 (2C), 21.3, 21.1 (3C), 21.0; elemental analysis calcd (%) $C_{58}H_{52}O_{16}$: C 69.3, H 5.2, found C 69.2, H, 5.0. HRMS [M + Na^+] m/z calcd for $C_{58}H_{52}O_{16}Na$ 1027.3148, found 1027.3110. ^{1}H and ^{13}C NMR spectra of *MM*-**5** and *PP*-**5** are similar to that of *rac*-**5.**

(17) Frisch, M. J.; et al. *Gaussian 03*, revision B.04; Gaussian Inc.: Pittsburgh, PA, 2003.

Synthesis of *rac*-1, *MM*-1 and *PP*-1 from Cryptophanes 5. *Rac*-**5** (0.18 g, 0.18 mM) was added to a mixture of THF (7 mL) and KOH (1M, 8 mL). The solution was stirred overnight at 60 °C under an argon atmosphere. THF was removed by rotary evaporation. Water (5 mL) was added and the solution was acidified with conc. HCl at 0 °C. The resulting precipitate was collected on a frit, washed with water and dried in air. The solid was washed successively with diethyl ether, a mixture of CH_2Cl_2 and Et_2O (50/50) and then with diethyl ether to provide clean *rac*-**1** (91% yield). Using the same synthetic route *MM*-**1** (76% yield) and *PP*-**1** (82% yield) were obtained from *PP*-**5** and *MM*-**5**, respectively. Mp (decomp) > 300 °C. ^{1}H NMR (500 MHz, KOD (0.08 M), 25 °C) δ 7.09 (d, ^{1}H, ^3J(H,H) = 8.4 Hz; Ar), 7.03 (s, 1H; Ar), 6.88 (s, 1H; Ar), 6.87 (d, 1H, ^3J(H,H) = 8.4 Hz; Ar), 6,86 (s, 1H; Ar), 6.78 (s, 2H; Ar), 6.75 (s, 1H; Ar), 6.71 (s, 1H; Ar), 6.59 (s, 1H; Ar), 6.57 (s, 1H; Ar), 6.51 (s, 1H; Ar), 4.70−4.60 (m, 1H; CH_2), 4.60−4.25 (m, 16H; H_a and CH_2), 4.08 (m, 1H, CH_2), 3,40 (d, 1H, ^2J(H,H) = 14.0 Hz; H_e), 3.32 (d, 1H, ^2J(H,H) = 13.5 Hz; H_e), 3,25 (d, 2H, ^2J(H,H) = 13.0 Hz; He), 3.20 (d, 2H, ^2J(H,H) = 13,5 Hz, He). ^{1}H NMR (500 MHz, DMSO; 25 °C) δ 8.69 (s, 1H; OH), 8.64 (s, 1H; OH), 8.59 (s, 12H; OH), 8.40 (s, 1H; OH), 8.30 (s, 1H; OH), 7.04 (d, 1H, ^3J(H,H) = 8.4 Hz, Ar), 6.73 (s, 1H; Ar), 6.66 (s, 1H; Ar), 6.64 (s, 1H; Ar), 6.635 (s, 1H; Ar), 6.59 (s, 3H, Ar), 6.58 (s, 1H; Ar), 6.56 (s, 1H; Ar), 6.54 (s, 1H; Ar), 6.50 (s, 1H; Ar), 6.45 (d, 1H, ^3J(H,H) = 8.4 Hz; Ar), 4.55 (d, 1H, ^2J(H,H) = 13.0 Hz; H_a), 4.42 (d, 1H, ^2J(H,H) = 13.0 Hz; H_a), 4.39 (d, 3H, ^2J(H,H) = 13.0 Hz; H_a), 4.38 (d, 1H, ^2J(H,H) = 13.0 Hz; H_a), 4.25−4.10 (m, 7H; CH_2), 4.10−3.90 (m, 5H; CH_2), 3.16 (d, 5H, ^2J(H,H) = 13.0 Hz; H_e), 3.14 (d, 1H, ^2J(H,H) = 13.0 Hz; H_e). ^{13}C NMR (125.76 MHz, DMSO, 25 °C) δ 155.4, 146.6, 146.3 (2C), 146.0, 145.0, 144.8, 144.7, 144.5, 144.2, 144.0, 140.5, 134.2, 134.0 (2C), 133.6, 132.7, 131.6, 130.8, 130.6, 130.2, 130.0, 129.7, 129.6, 121.2, 120.3, 120.0, 119.7, 117.7, 117.6, 117.4, 117.2 (2C), 116.6, 116.3, 111.2, 69.0, 68.9, 68.8, 68.6, 64.8, 64.6, 35.5, 35.1, 35.0 (2C), 34.9, 34.6; HRMS [M + Na^+] m/z calcd for $C_{48}H_{42}O_{11}Na$ 817.2619, found 817.2612. ^{1}H and ^{13}C NMR spectra of *MM*-**1** and *PP*-**1** are similar to that of *rac*-**1**.

Acknowledgment. The authors are indebted to the CNRS (Chemistry Department) and to Région Aquitaine for financial support in FTIR and optical equipments. They also acknowledge computational facilities provided by the Pôle Modélisation of the Institut des Sciences Moléculaires and the M3PEC-Mésocentre of the University Bordeaux 1 (http://www.m3pec.u-bordeaux1.fr), financed by the Conseil Régional d'Aquitaine and the French Ministry of Research and Tecnology. Finally, support from the French Ministry of Research (ANR project NT09-472096 GHOST) is acknowledged.

Supporting Information Available: ^{1}H NMR and ^{13}C NMR spectra of *rac*-**5** in CD_2Cl_2 solution. ^{1}H NMR spectra of *MM*-**1** and *PP*-**1** in D_2O/KOD solution (0.08 M). ^{13}C NMR spectrum of *MM*-**1** in DMSO-*d6* solution. UV−vis spectra of empty *rac*-**1** as well as *rac*-**1** in presence of CH_2Cl_2 and $CHCl_3$ in H_2O/LiOH, H_2O/NaOH, H_2O/KOH and H_2O/CsOH solutions (0.1 M). ECD spectra of *MM*-**1** in NaOH aqueous solutions at different pH values. ECD spectra of *MM*-**1** in H_2O/NaOH (0.1 M) and MeOH solutions. ECD spectra of empty *PP*-**1** as well as *PP*-**1** in presence of Xe, CH_3Cl, CH_3I, CH_2BrCl, CH_2Br_2 and CH_2ClI in H_2O/NaOH solution (0.1M). ECD spectra of empty *PP*-**1** as well as *PP*-**1** in presence of Xe, CH_3Cl, CH_3I, CH_2BrCl and CH_2Br_2 in H_2O/LiOH solution (0.1M). IR spectra of *rac*-**1** in D_2O/KOD and D_2O/CsOD solutions at different concentrations. IR and VCD spectra of empty *PP*-**1** as well as *PP*-**1** in presence of xenon, CD_2Cl_2 and $CDCl_3$ in D_2O using KOD and

CsOD solutions (0.21 M). ^{1}H NMR (500 MHz) spectra of empty *rac*-**1** as well as *rac*-**1** in presence of CH_2Cl_2 recorded at 278 K in D_2O/KOD. Distance between the center of the cavity and the sodium (or cesium) cations, extracted from MD calculations of empty *PP*-**1**. ECD spectra of empty *MM*-**1** in H_2O/CsOH solution (0.1 M) as well as *MM*-**1** in H_2O/LiOH (0.1 M) + CsOH (2×10^{-4} M) solution in presence (saturated solution) or not of $CHCl_3$. Full list of authors of reference 17. This material is available free of charge via the Internet at http://pubs.acs.org.